JBC RESEARCH ARTICLE

PTEN-induced kinase PINK1 supports colorectal cancer growth by regulating the labile iron pool

Received for publication, October 1, 2022, and in revised form, April 1, 2023 Published, Papers in Press, April 8, 2023,
https://doi.org/10.1016/j.jbc.2023.104691

Brandon Chen[1], Nupur K. Das[1], Indrani Talukder[1], Rashi Singhal[1], Cristina Castillo[1], Anthony Andren[1], Joseph D. Mancias[2], Costas A. Lyssiotis[1,3,4,*], and Yatrik M. Shah[1,3,4,*]

From the [1]Department of Molecular and Integrative Physiology, University of Michigan, Ann Arbor, Michigan, USA; [2]Division of Radiation and Genome Stability, Department of Radiation Oncology, Dana-Farber Cancer Institute, Harvard Medical School, Boston, Massachusetts, USA; [3]University of Michigan Rogel Cancer Center, and [4]Department of Internal Medicine, University of Michigan, Ann Arbor, Michigan, USA

Reviewed by members of the JBC Editorial Board. Edited by Donita Brady

Mitophagy is a cargo-specific autophagic process that recycles damaged mitochondria to promote mitochondrial turnover. PTEN-induced putative kinase 1 (PINK1) mediates the canonical mitophagic pathway. However, the role of PINK1 in diseases where mitophagy has been purported to play a role, such as colorectal cancer, is unclear. Our results here demonstrate that higher PINK1 expression is positively correlated with decreased colon cancer survival, and mitophagy is required for colon cancer growth. We show that doxycycline-inducible knockdown (KD) of PINK1 in a panel of colon cancer cell lines inhibited proliferation, whereas disruption of other mitophagy receptors did not impact cell growth. We observed that PINK KD led to a decrease in mitochondrial respiration, membrane hyperpolarization, accumulation of mitochondrial DNA, and depletion of antioxidant glutathione. In addition, mitochondria are important hubs for the utilization of iron and synthesizing iron-dependent cofactors such as heme and iron sulfur clusters. We observed an increase in the iron storage protein ferritin and a decreased labile iron pool in the PINK1 KD cells, but total cellular iron or markers of iron starvation/overload were not affected. Finally, cellular iron storage and the labile iron pool are maintained *via* autophagic degradation of ferritin (ferritinophagy). We found overexpressing nuclear receptor coactivator 4, a key adaptor for ferritinophagy, rescued cell growth and the labile iron pool in PINK1 KD cells. These results indicate that PINK1 integrates mitophagy and ferritinophagy to regulate intracellular iron availability and is essential for maintaining intracellular iron homeostasis to support survival and growth in colorectal cancer cells.

Mitochondria are critical metabolic organelles that sustain cellular bioenergetics and biosynthetic needs (1). The electron transport chain (ETC) integrates central carbon metabolism and redox homeostasis to support metabolic demands of the cells. To maintain a healthy mitochondrial network, organellar functions are continuously monitored *via* quality control mechanisms (2). Dysfunctional mitochondria are turned over by a cargo-specific, lysosomal-dependent, autophagic degradation mechanism termed mitophagy (3). Dysregulation of mitophagy is associated with progression of several cancers (4). Parkin-induced protein kinase 1 (PINK1) is a sensor of mitochondrial health, and activation of PINK1 regulates one of the most well-defined mitophagy pathways (5, 6). However, the role of PINK1 as a tumor suppressive surveillance mechanism for enhancing survival and proliferation are context dependent (7–9).

Induction of PINK1-mediated mitophagy is triggered by the loss of membrane potential from uncoupling the proton or potassium gradient (10). Recent results illustrated that chelation of mitochondrial iron potently induced mitophagy (11).The role of mitochondria in iron metabolism is well established. The synthesis of iron sulfur cluster (Fe-S) and heme is initiated in the mitochondria. Moreover, mitochondria ETC require Fe-S cluster and heme-containing protein such as cytochrome c to facilitate electron transfer. However, the exact mechanism linking the loss of mitochondrial iron and mitophagy is not yet fully understood (11, 12).

In excess, iron is cytotoxic to cells. Cellular iron levels are balanced by an intricate network of regulatory mechanisms. A central protein in iron handling is the iron storage protein ferritin (FTN). A study demonstrates that following uptake, iron goes through a transient FTN intermediate to prevent oxidative damage (13). Subsequently, FTN-bound iron release is mediated by autophagic degradation of nuclear receptor coactivator 4 (NCOA4) in a process termed ferritinophagy. Following FTN degradation, lysosomal/endosomal iron can be distributed in the cell *via* direct lysosome-organelle contacts or chaperones (14, 15). As an example, recent studies demonstrated that iron turnover from ferritinophagy is critical to support mitochondrial iron sulfur cluster biogenesis and respiration in pancreatic cancer (16, 17).

To study the connection between mitophagy and iron balance, we generated a genetic, PINK1 loss-of-function model in colorectal cancer (CRC) cells. We identified PINK1-mediated mitophagy as a critical pathway for CRC cell proliferation and mitochondrial function. The loss of PINK1 led to

* For correspondence: Yatrik M. Shah, shahy@umich.edu; Costas A. Lyssiotis, clyssiot@med.umich.edu.

increased sequestration of labile iron in FTN. The proliferative defects and cellular labile iron pool (LIP) in PINK1 knockdown (KD) was rescued by activating ferritinophagy *via* nuclear receptor coactivator 4 (NCOA4) overexpression. Overall, our study suggests that disruption of the canonical mitophagy pathway contributes to cytosolic iron imbalance, which can be rescued by activating ferritinophagy.

Results

PINK1 is required for CRC proliferation in vitro *and* in vivo

We demonstrated that CRC cells utilize mitophagy to support metabolic rewiring under nutrient-deprived conditions (18). We generated Kaplan–Meier plots from published transcriptomic data from colon cancer patients. We stratified gene expression data into high and low PINK1 expression based on median expression and compared regression-free survival over a span of 200 months. Log-ranked test indicated a significant *p*-value of $1.6e^{-5}$. Moreover, the hazard ratio analyses revealed improved survival of patients with low PINK1 expression level (Fig. 1*A*). In addition, mining the Human Protein Atlas, CRC cells robustly express PINK1 compared to several other cancers (Fig. 1*B*). We generated two independent doxycycline (DOX)-inducible shRNA targeting PINK1 (19). To test cell proliferation and viability, we counted cell number over time to account for proliferation and utilized colony formation assay to assess the ability of cells to form single unit colonies. When assessing growth differences between WT and PINK1 KD, we compared DOX-treated groups of shNT *versus* shPINK1 instead of between isogenic shPINK1 cells with and without DOX. In this study, we focused on two human CRC cell lines, HCT116 and SW480, which are widely used for colon cancer. The genomic profiles of these cell lines are well characterized, featuring activating KRAS mutations, which are representative of a significant proportion of mutations observed in CRC patients. Additionally, we generated shRNA constructs in a panel of other human and mouse CRC cell lines. Upon PINK1 KD, we observed proliferative defects and decreased colony-forming capacity in several CRC cell lines (HCT116, SW480, RKO, HT29, MC38, CT26) (Fig. 1, *C* and *D*). KD was validated by decreased PINK1 mRNA transcript (Fig. S1*A*). However, disruption of PINK1-independent mitophagy executors, parkin, BNIP3, NIX, FUNDC1, did not exhibit growth defects (Fig. S1, *B* and *C*). In addition, analysis of PINK1 KD cells in a subcutaneous xenograft model revealed decreased tumor burden with decreased tumor volume, tumor weight, and proliferation

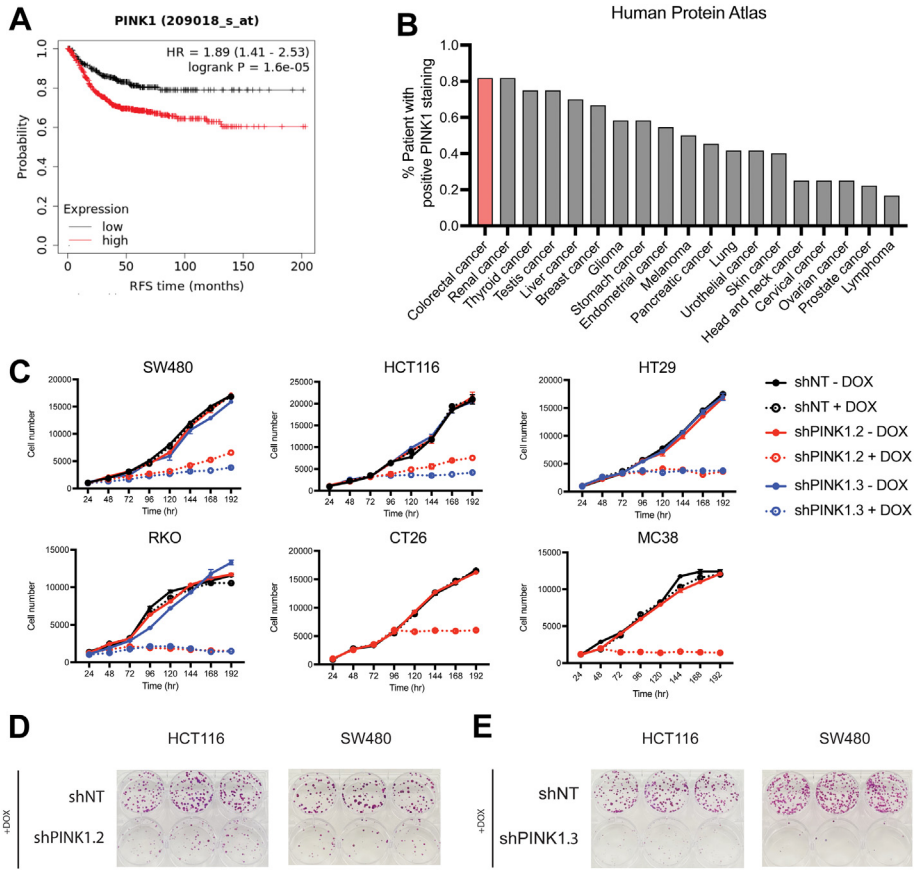

Figure 1. PINK1 is associated with poor patient survival and required for colorectal cancer's *in vitro* growth. *A*, microarray data on colorectal cancer patient regression free survival stratified based on median PINK1 expression. *B*, Human Protein Atlas (HPA) data on % patient with positive PINK1 expression (accession number HPA00193). Human colorectal cell lines (HCT116, SW480, HT29, RKO) and mouse colorectal cancer cell lines (CT26 and MC38) with doxycycline-inducible nontargeting (shNT) and two independent shRNA targeting PINK1 (shPINK1.2 and shPINK1.3; only shPINK1.2 is compatible with mouse PINK1 mRNA sequence). 50 ng/ml of doxycycline were used for (*C*) cell proliferation and (*D*) and (*E*) colony formation assays. (mean −/+ SEM, N = 3 per condition). HR, hazard ratio; RFS, regression free survival.

and increased TUNEL staining following DOX treatment (Fig. 2, *A–D*). This data demonstrates that PINK1 has an essential role in mediating CRC cell growth.

Inhibition of PINK1 disrupts mitophagy and mitochondrial functions

Mitophagy is the process by which damaged mitochondria are degraded and the components are recycled to support cell growth. Upon loss of mitochondrial membrane potential, PINK1 accumulates on the outer mitochondrial membrane (OMM) and recruits E3 ligase Parkin to coordinate the decoration of OMM and OMM proteins with phospho-ubiquitin (pUb) chains (20). pUb chains subsequently recruit autophagic adaptors such as p62 to deliver mitochondria to autophagosomes for degradation (11). PINK1 KD prevented accumulation of pUb in response to carbonyl cyanide m-chlorophenylhydrazone, a mitochondrial uncoupler (19) (Fig. 3*A*). In addition, we sought to characterize mitophagy flux utilizing a mitochondrially targeted tandem Cox8-mCherry-GFP mitophagy reporter (21) (Fig. 3*B*). GFP is a pH-sensitive fluorophore, while mCherry is pH-insensitive. Upon the internalization of mitochondria into the acidic autophagosome, the localized GFP signal is quenched, whereas mCherry will remain fluorescent. PINK1 KD effectively decreased mitophagy flux (Fig. 3*C*). Moreover, we observed an increase in mitochondrial DNA content, which indicated accumulation of mitochondria (Fig. 3*D*).

Next, mitochondrial function was investigated following PINK1 KD. Seahorse analysis demonstrated lower basal oxygen consumption rate (OCR) and maximal respiration in PINK1 KD cells (Figs. 3*E* and S2, *A* and *B*). ETC is tightly coupled with mitochondrial membrane potential, and PINK1 KD cells had increased mitochondrial membrane potential, which is indicative of mitochondrial hyperpolarization. Previously, mitochondria hyperpolarization has been shown to occur under chronic inhibition of ETC CI inhibition and reduced CII, CIII, and CIV activity (22) (Fig. 3*F*). Mitochondrial ETC complex I is also required to oxidize NADH to sustain NAD pools. We observed elevated levels of NADH/NAD ratio upon PINK1 KD (Fig. 3*G*).

Cellular redox balance and nucleotide metabolism are disrupted upon PINK1 inhibition

Mitochondria integrate the metabolism of nutrients such as glucose, glutamine, and fatty acids to coordinate

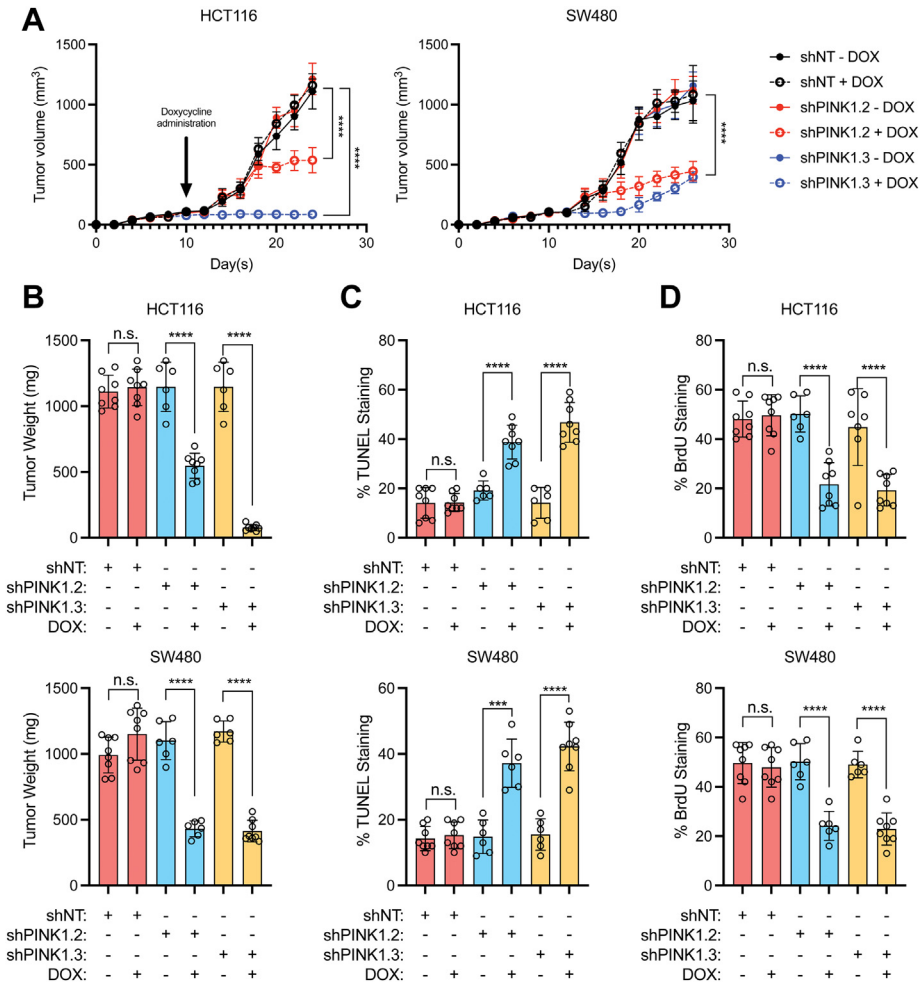

Figure 2. PINK1 is required for colorectal cancer's *in vivo* growth. *A*, HCT116 and SW480 shNT, shPINK1.2, and shPINK1.3 tumor were injected into the flanks of NOD/SCID mice to measure tumor volume over time with or without doxycycline (DOX) chow. *B*, endpoint tumor weight was measured. *C*, percent (%) TUNEL staining and (*D*) BrdU staining was quantified. *** indicates $p < 0.0005$, **** indicates $p < 0.0001$. (mean −/+ SEM, N = 6 or 8 per condition).

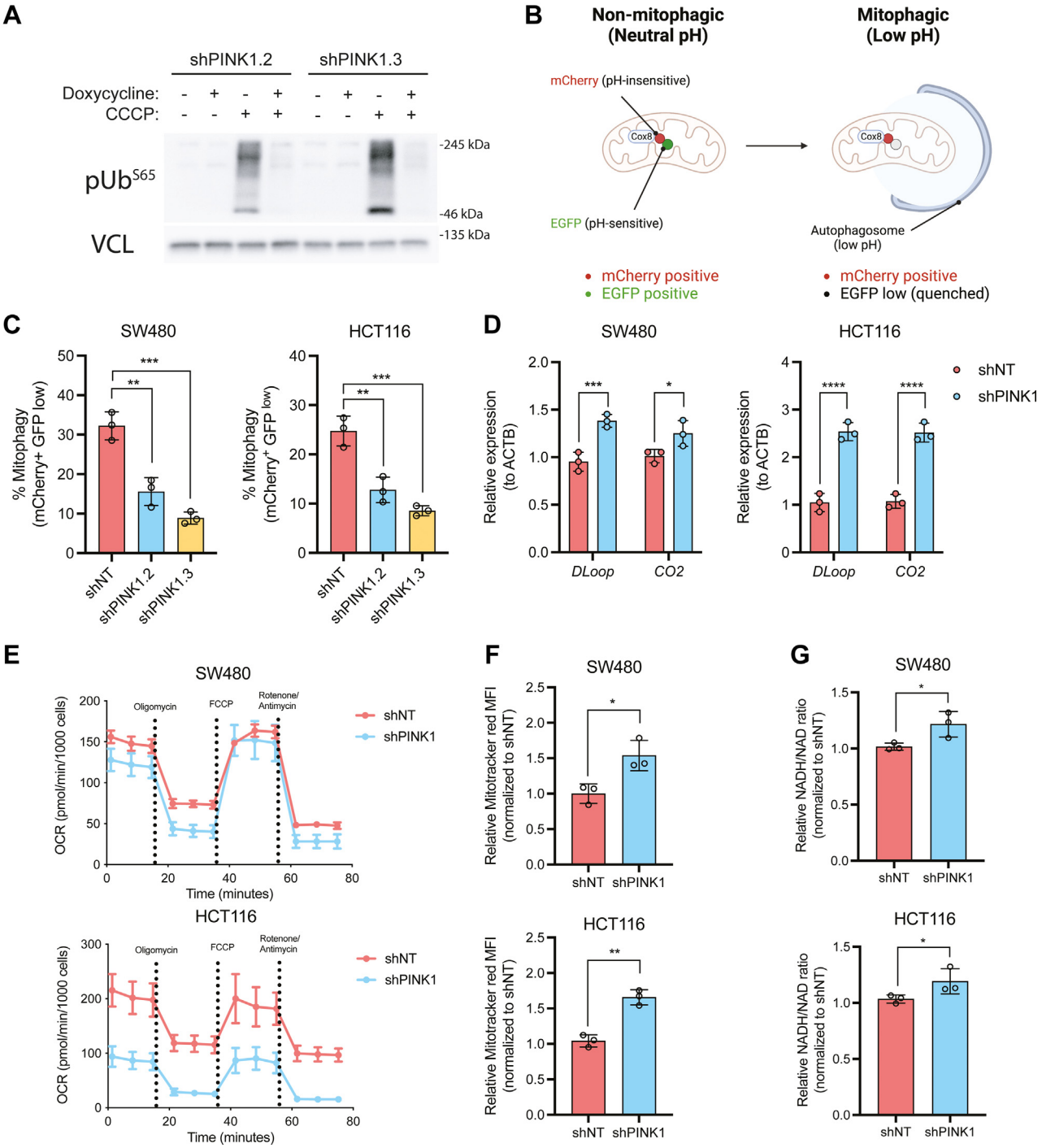

Figure 3. Loss of PINK1 disrupts mitophagy and contributes to mitochondrial dysfunction. *A*, infographic of the COX8-EGFP-mCherry mitophagy reporter. *B*, mitophagy flux was measured using the aforementioned reporter. *C*, cells were treated with vehicle or 10 μM CCCP, and phosphorylated ubiquitin (pS65-Ub) was immunoblotted for PINK1 activity. *D*, mtDNA content is assessed using mitochondrially encoded gene D-Loop and cytochrome c oxidase 2 (CO2). *E*, Seahorse Mito Stress Test was conducted with following order and concentration of inhibitors: oligomycin (1 μM), FCCP (1 μM), rotenone (1 μM), and antimycin A (1 μM). (mean −/+ SEM, N = 4 per condition). *F*, mitochondrial membrane potential is measured by Mitotracker Red CMXRos. *G*, relative NADH/NAD ratio. * indicates $p < 0.05$, ** indicates $p < 0.001$, *** indicates $p < 0.0005$, **** indicates $p < 0.0001$. CCCP, carbonyl cyanide m-chlorophenylhydrazone; mtDNA, mitochondrial DNA.

energy production, the regulation of redox homeostasis, and other biosynthetic precursors. Liquid chromatography tandem mass spectrometry–based metabolomics was used to profile changes in central carbon metabolism upon PINK1 KD. Here, we observed a downregulation of the reduced glutathione (GSH) to oxidized glutathione (GSSG) ratio and nucleotides (*i.e.* ADP, AMP, UDP, IMP) in SW480 (Fig. 4, *A* and *B*, and Table S1). Together with the bioenergetic profiling data in Figure 2, this evidence indicates that losing the ability to recycle mitochondria *via*

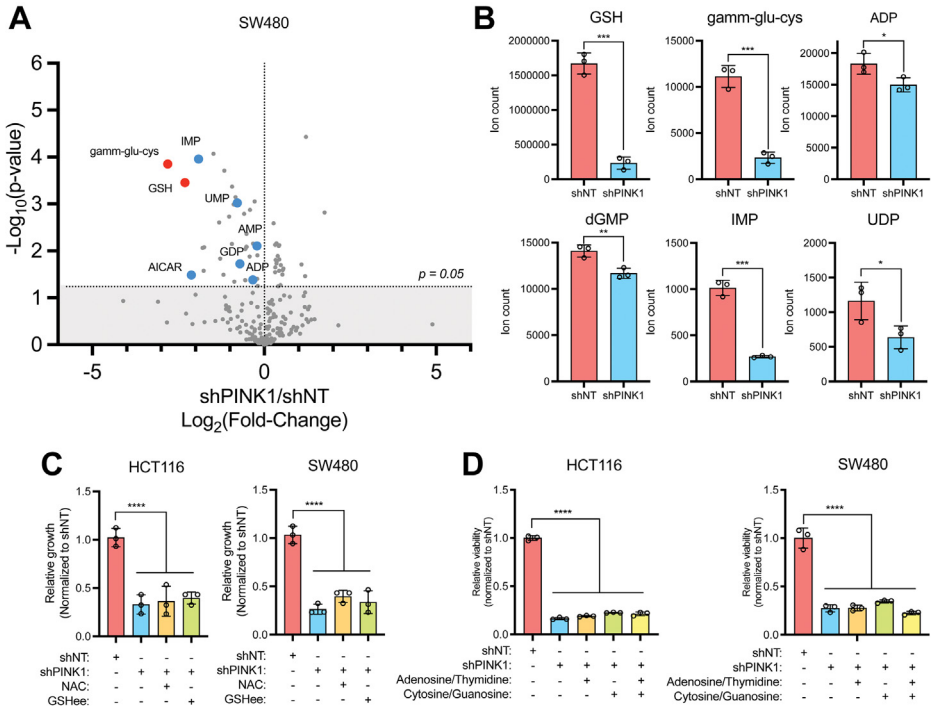

Figure 4. Disruption of redox and nucleotide metabolism is secondary to PINK1-dependent growth defects. *A*, metabolite profiling *via* mass spectrometry–based metabolomics were conducted on both cell lines 3 days after induction of shNT and shPINK1. n = 3 for collected metabolite samples. *B*, selected metabolites associated with redox and nucleotides from SW480 were shown to decrease under PINK1 knockdown. *C*, cells were treated with 1 mM NAC and GSHee. *D*, cells were treated with 100 μM adenosine/thymidine or cytosine/guanosine. * indicates $p < 0.05$, ** indicates $p < 0.001$, *** indicates $p < 0.0005$, **** indicates $p < 0.0001$. (mean −/+ SEM, N = 3 per condition). GSHee, glutathione ethyl ester; NAC, N-acetylcysteine.

PINK1-dependent mitophagy inhibits mitochondrial respiration and contributes to cellular metabolic dysfunction.

To reverse proliferation defects that resulted from PINK1 KD, based on our metabolomics data, we supplemented cells with the antioxidants N-acetylcysteine or glutathione ethyl ester, or the nucleosides (adenosine, thymidine, cytosine, and guanosine) (Fig. 4, *C* and *D*). However, these metabolites did not rescue the growth defects in PINK1 KD cells. To resolve elevated NADH/NAD ratio, we employed *Lactobacillus brevis* NADH oxidase (*Lb*NOX) and mitochondrial targeted LbNOX (mt*Lb*NOX), which oxidize NADH to water, in order to determine the impact of reductive stress on our PINK1 KD phenotype. Here too, we failed to rescue PINK1 KD (23) (Fig. S2*A*). Additionally, the NADH buildup from defective ETC complex I can be rescued by expression of a yeast version of NADH oxidase, NDI1 (24). NDI1 rescued phenformin-dependent proliferative defect; it did not rescue proliferation in PINK1 KD cells. This demonstrates that increasing the oxidation of NADH is not sufficient to restore PINK1-dependent proliferative defects (Fig. S2*E*). Lastly, the pan-caspase/apoptosis inhibitor (z-VAD-FMK), ferroptosis inhibitor (Ferrostatin 1; Fer1), and necroptosis inhibitor (Necrostatin 1; Nec1) did not reverse growth defects in PINK1 KD cells (Fig. S2*B*). Collectively, these data suggested that metabolic dysregulation was secondary of the growth suppressive and mitochondrial dysfunction phenotypes following PINK1 KD.

PINK1 modulates intracellular iron distribution independent of the canonical iron starvation response

In addition to their above noted role in metabolism, mitochondria are also important hubs for cellular iron utilization. Iron sulfur clusters (Fe-S) and heme biosynthetic pathways initiate in the mitochondria. Iron and iron-containing cofactors are critical for electron transport and redox balance as iron is a redox active element that can shuttle electrons along the respiratory chain. Moreover, we have shown that nucleotide metabolism requires iron for pyrimidine/purine biosynthesis (25). Acute depletion of mitochondrial iron *via* deferiprone induces mitophagy, thus linking mitochondrial turnover to cellular iron homeostasis (11). To measure the mitochondrial iron pool, we utilized a flow cytometry–compatible mitochondrial iron stain, Mito-FerroGreen. With this, we observed that PINK1 KD decreased mitochondrial iron levels (Fig. 5*A*).

Mitochondrial iron is sensitive to cytosolic iron perturbation. For example, extracellular iron depletion induces hypoxia-inducible factor and thus drives the expression of mitochondrial iron transport SLC25A37 (26, 27). Cells have an extensive regulatory network that monitors iron homeostasis (28). Excess cytosolic LIP can lead to oxidative damage (29, 30). Thus, iron is tightly regulated through many overlapping and distinct pathways. FerroOrange measures total LIP, which was robustly decreased upon PINK1 KD (Fig. 5*B*). In contrast, total cellular iron was not changed, as assessed by inductively-coupled plasma mass spectrometry (ICP-MS), as well as other

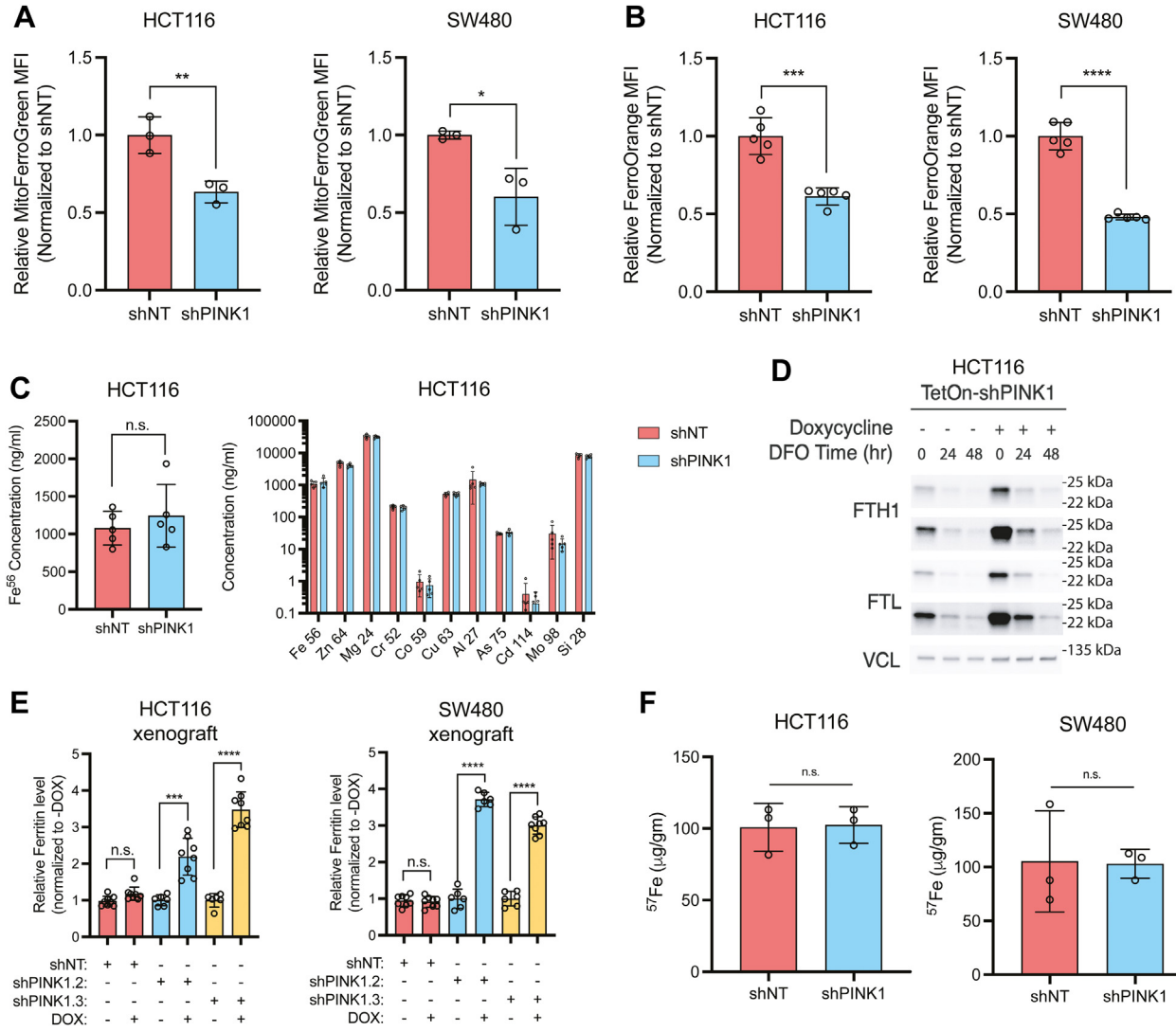

Figure 5. PINK1 modulate intracellular iron distribution independent of canonical iron starvation response. *A*, Mito-FerroGreen– (MFG) and (*B*) FerroOrange-stained shNT and shPINK1 cells were subjected to flow cytometry analyses of mean fluorescence intensity (MFI). *C*, ICP-MS analyses of divalent metals and iron (Fe56) in shNT and shPINK1 cells. *D*, immunoblotting of WT and shPINK1 cells treated with 100 µM of deferoxamine (DFO) for 24 and 48 h (mean −/+ SEM, N = 5 per condition). *E*, ELISA measurement of ferritin from xenograft model of shNT and shPINK1 HCT116 and SW480 cells (described in Fig. 2). *F*, stable iron isotope (57Fe) uptake from WT and shPINK1 cells treated with 100 µM of ^{57}Fe for 2 h * indicates $p < 0.05$, ** indicates $p < 0.001$, *** indicates $p < 0.0005$,**** indicates $p < 0.0001$. ICP-MS, inductively-coupled plasma mass spectrometry.

trace metal elements (Fig. 5*C*). High levels of iron lead to the upregulation of the iron storage protein FTN expression and stabilization, which is composed of FTN heavy chain (FTH1) and FTN light chain (FTL). FTN sequesters excessive iron, preventing cellular oxidative damage from excessive LIP. In PINK1 KD cells, increased FTH1 and FTL was observed (Fig. 5*D*). FTN accumulation observed in PINK1 KD cells is consistent in our subcutaneous xenograft tumors (Fig. 5*E*).

The regulation of cellular iron homeostasis involves transferrin receptor–mediated iron uptake, endolysosomal trafficking and release, and posttranscriptional regulation of iron-related mRNA transcripts by iron response protein 2 (31). We observed an increase in transferrin receptor expression in PINK1 KD HCT116, but there was no change in SW480. Iron response protein 2 level was also not altered upon PINK1 KD in both cell lines. To determine if cellular iron uptake is increased in PINK1 KD cells, the cells were treated with a heavy iron-^{57}Fe isotope. Cellular iron-^{57}Fe was measured by ICP-MS, and no change in iron uptake was observed (Figs. 5*F* and S3*A*). These data together suggest that canonical iron starvation response is not involved in PINK1-dependent FTN regulation.

Restoring iron homeostasis via *NCOA4-mediated ferritinophagy reverses growth suppression upon PINK1 inhibition*

To understand the role of iron in the growth defects following PINK1 KD, we supplemented with ferric ammonium citrate (FAC) to rescue LIP and mitochondrial iron. Interestingly, growth was not rescued in the PINK1 KD cells (Fig. 6*A*). An increase in FTN levels upon FAC treatment was observed, but no increase in LIP or mitochondrial iron, indicating that introduction of exogenous iron was primarily integrated to

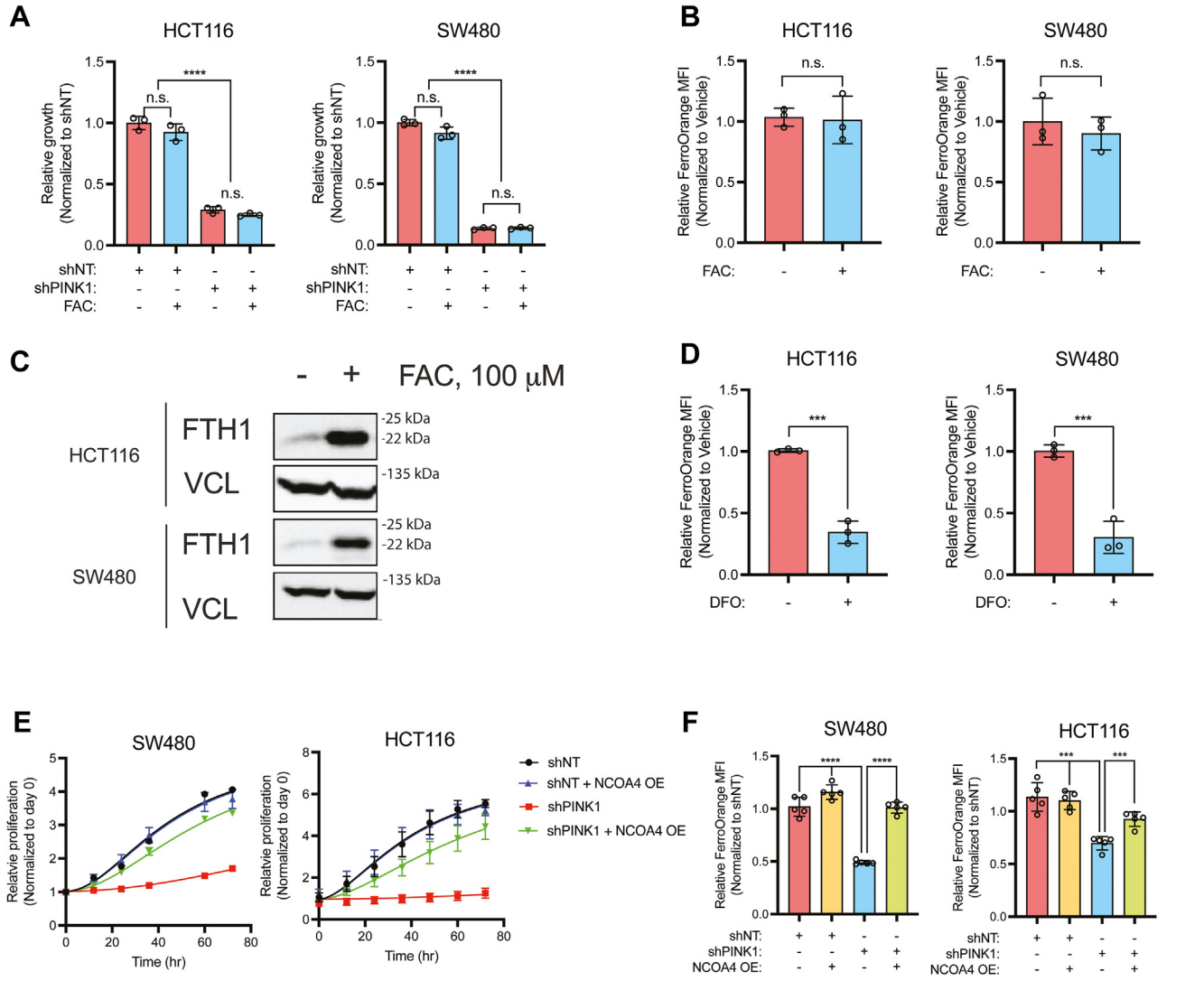

Figure 6. Restoring iron homeostasis *via* NCOA4-mediated ferritinophagy reverse growth suppression role of PINK1 loss. *A*, shNT and shPINK1 cells were treated with 100 μM ferric ammonium citrate (FAC), and proliferation was measured for 72 h. *B*, WT HCT116 and SW480 were treated with 100 μM FAC for 72 h for FerroOrange measurement. *C*, immunoblot of ferritin (FTN) upon 24 h 100 μM FAC treatment. *D*, measurement of LIP with FerroOrange upon DFO treatment. *E*, Cell number was monitored for NCOA4 overexpression in shNT and shPINK1 cells. *F*, FerroOrange labile iron stain mean fluorescence intensity (MFI) was measured and normalized to shNT. (mean −/+ SEM, N = 3 or five per condition). *** indicates $p < 0.0005$, **** indicates $p < 0.0001$. The significance between *green* and *red dot* is ****. DFO, deferoxamine; LIP, labile iron pool.

FTN complexes (Fig. 6, *B* and *C*). Indeed, iron chelation with deferoxamine (DFO) decreased LIP (Fig. 6*D*). Cells compensate for the loss of cellular LIP *via* a cargo-specific autophagic degradation of FTN by ferritinophagy (32, 33). We show that DFO depleted FTN levels in WT cells, but PINK1 KD maintained higher FTN levels (Fig. 5*D*). This data suggested that there are defects in ferritinophagy that decrease LIP in the PINK1 KD cells.

Ferritinophagy is coordinated by the cargo receptor NCOA4, which binds to both FTL and FTH1 and delivers FTN to autophagosomes for degradation and release of iron (33). In addition to liberating FTN-bound iron for other iron-dependent processes, NCOA4 has been reported to be important for mitochondrial iron balance and respiration (34). To rescue FTN accumulation in PINK1 KD cells, NCOA4 was over expressed (Fig. S3*B*). NCOA4 expression was sufficient to rescue proliferative defects of PINK1 KD and restore LIP in these cells (Fig. 6, *E* and *F*). Overall, here we demonstrated that PINK1 loss leads to mitochondrial dysfunction and iron accumulation in FTN. Liberating the sequestered iron from the FTN complex by inducing ferritinophagy was able to compensate for PINK1 KD. This data suggests an essential role of mitophagy in regulating the LIP *via* ferritinophagy.

Discussion

Mitochondria are important biosynthetic and metabolic hubs in tumorigenesis. Functional mitochondria are critical to support cancer cell growth (35). Stressors in the tumor microenvironment such as hypoxia and nutrient dysregulation and intrinsic factors driving mitochondrial DNA heteroplasmy require adaptations to mitochondrial dynamics, turnover, and programs for cancer cell survival (36, 37). The induction of mitophagy requires exogenous expression of parkin and

mitochondrial damage to remove the mitochondrial pool (38). Mitophagy is essential in colon cancer growth, however, the underlying mechanisms are unclear. The present work demonstrates that inhibition of PINK1-mediated mitophagy decreases colon cancer growth in a panel of colon cancer-derived cell lines. CRC cells have high basal mitophagy (18), and failure to execute mitophagy leads to proliferative defects. Mechanistically, we show that colon cancer cells are dependent on PINK1 to maintain mitochondrial respiration. Although we did observe metabolite changes such as decreased reduced glutathione and several nucleotide species, rescue with these metabolites was not sufficient to restore PINK1-dependent proliferative defects. Rather, we demonstrate that PINK1 KD decreases the LIP, and restoring ferritinophagy was sufficient to rescue cell proliferation (Fig. 7).

The critical role of mitochondria in iron homeostasis is well appreciated. Mitochondrial uptake of iron *via* the mitoferrins (SLC25A28/37) is essential for the biosynthesis of iron sulfur clusters proteins and heme (39). Iron sulfur clusters and heme are both important cofactors that support ETC, nucleotide biosynthesis, and DNA replication (40). Although iron is a critical micronutrient essential for many biological processes, excessive free iron can be cytotoxic and exert oxidative stress (41). Therefore, the balance between iron storage in multimeric FTN complexes and FTN turnover *via* ferritinophagy is tightly regulated. In addition to its role in FTN turnover, NCOA4 is involved in packaging FTN into extracellular vesicles (42). This may explain the observed increase in cellular FTN levels. However, our data show that even after DFO treatment, FTN levels remain elevated, indicating a cellular dysfunction in FTN metabolism. Further research is needed to determine if PINK1 KD also affects the packaging of FTN into extracellular vesicles. The ferritinophagy adaptor NCOA4 has also been implicated in mitochondrial iron balance (34). However, the canonical mitophagy pathway driven by PINK1 and how this cross talks with cellular iron homeostatic mechanisms are still unclear.

The most well-studied PINK1 substrates include the mitochondrial outer membrane proteins mitofusins (MFN1/2), ubiquitin, and parkin (43). The phosphorylation targets downstream of PINK1 activation are often signals that recruit autophagy adaptors to deliver mitochondria to autophagosomes. The kinase domain of PINK1 faces the cytosolic side and is postulated to have targets outside of OMM proteins (44). Interestingly, phosphorylation targets for PINK1 were identified under mitochondrial uncoupled conditions. However, our study pinpoints a role of homeostatic PINK1 in CRC cells. This distinction may alter the subset of proteins targeted by PINK1 basally. Although mitophagy and ferritinophagy are distinct cargo-selective autophagic pathways, several players in these two pathways are shared (45). We speculate that loss of PINK1 inhibits overlapping effectors that are central in mitophagy and ferritinophagy. Thus, future studies will be needed to identify relevant PINK1 targets and the complex

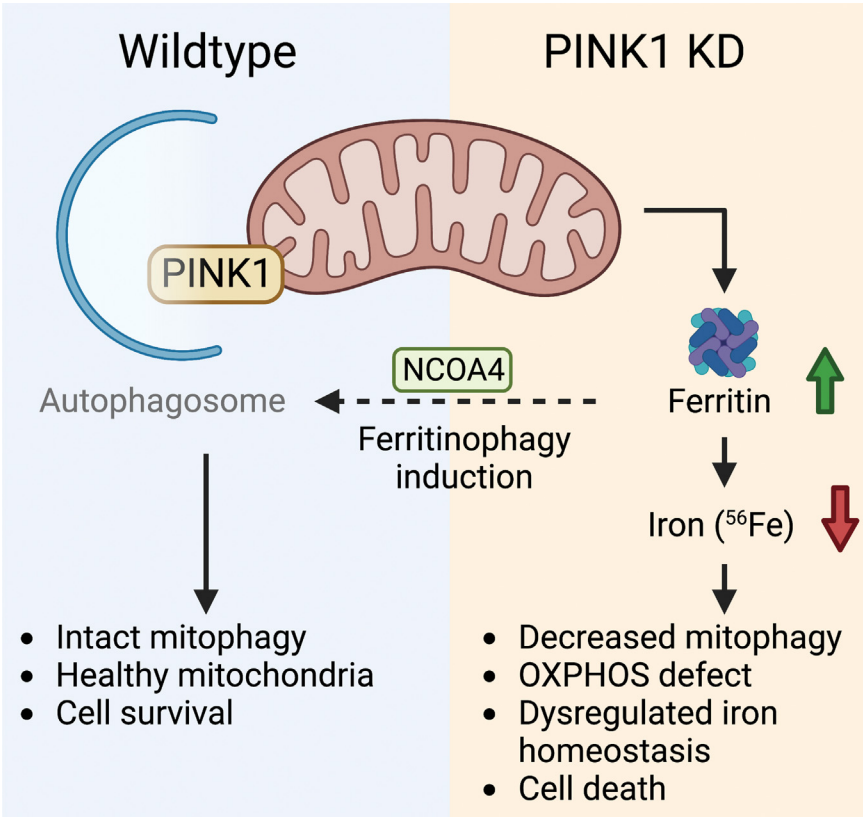

Figure 7. Schematic of PINK1-dependent iron toxicity in CRC cells. The data indicate that in PINK1-mediated mitophagy, ferritinophagy is necessary to sustain a dynamic iron pool. When PINK1 is knocked down (KD), the degradation of ferritin is hindered, resulting in a reduced level of labile iron leading to a decrease in cell growth. CRC, colorectal cancer.

interplay of various autophagy adaptors in balancing mitophagy and ferritinophagy.

Based on our study, we found that receptor-mediated mitophagy *via* BNIP3, NIX, and FUNDC1 does not play a significant role in CRC cell proliferation and survival. These receptors can directly target mitochondria for autophagic degradation without ubiquitination of OMM proteins. Despite the residual mitophagy activity sustained by BNIP3, NIX, and/or FUNDC1 following PINK1 KD, this is insufficient to sustain CRC survival in the absence of PINK1. Moreover, knockout of BNIP3, NIX, and FUNDC1 did not decrease CRC cell proliferation suggesting the dominant mitophagy pathway that supports CRC survival is PINK1-dependent. However, receptor-mediated mitophagy may become more important under hypoxia as both BNIP3 and NIX are regulated by hypoxia-inducible factor (46). FUNDC1 undergoes hypoxia-dependent dephosphorylation and activation by PGAM5 which promotes mitochondrial fission and mitophagy activation (47).

Mitochondrial quality control mechanisms, such as mitophagy, play a critical role in maintaining functional mitochondria. Upon PINK1 KD, we observed decreased oxygen consumption and mitochondrial membrane potential hyperpolarization. Our data suggest that respiratory chain defects are direct results from the inability of CRC cells to turnover aged and defective mitochondria. Without this ability, ETC proteins become dysfunctional due to oxidative damage. Previous studies demonstrate that loss of PINK1 leads to mitochondrial depolarization in mouse embryonic fibroblasts (10), but the outcome of mitochondrial membrane potential upon ETC dysfunction may vary in different cellular systems. This is due to the complex regulation of mitochondria membrane potential which includes the ability of the ETC to undergo CV reversal and conduct ATP hydrolysis, which is dependent on the expression of ATPIF1, as well as the ability of ANT to fuel the matrix with protons and ADP (22). It is difficult to determine if PINK1 is a positive or negative regulator of membrane potential. However, our findings show a connection between respiratory defects and mitochondrial hyperpolarization in the CRC cell models we studied.

We provide evidence of direct crosstalk between two cargo-specific autophagic pathways, mitophagy and ferritinophagy. This connection between mitochondrial quality control mechanism and iron homeostasis has been reported to mediate important cellular pathophysiology, but mechanistic insights have been lacking. A study suggested the possibility that NCOA4 recognizes mitochondrial FTN on the outer mitochondria membrane and directly degrading mitochondria *via* autophagy (12). However, we propose a potential alternative mechanism to their NCOA4-dependent mitophagy paradigm since mitochondrial FTN expression is undetectable in our CRC cell lines. Previous studies have identified that intestinal epithelial-derived cancer cells utilize mitophagy to evade T cell immunity *via* lysosomal iron overload (48). In addition, genetic deletion of PINK1 in pancreatic cancer contributes to mitochondrial iron overload *via* accumulation of mitochondrial iron importers (26). Since mitochondria can harbor abundant cellular iron, their roles in mediating iron storage and subcellular utilization have been increasingly scrutinized (49, 50). Moreover, colon cancer cells sequester iron to fuel prosurvival responses such as hypoxic signaling and nucleotide biosynthesis. Due to the redox reactivity of iron, iron mobilization is swiftly carried out by chaperones and compartmentalized by different organelles. Disruption of iron handling machineries has been implicated in cellular dysfunction. Loss of mitochondrial iron contributes to decreased oxygen consumption and respiratory chain defects.

Mitochondrial and FTN turnover coordinate dynamic responses central in sustaining CRC growth. Although there are no specific agents that specifically block mitophagy, hydroxychloroquine is a lysosomotropic agent that blocks all form of autophagy *via* neutralization of lysosomal pH and lysosome dysfunction. Hydroxychloroquine has demonstrated promising results in conjunction with standard chemotherapeutics in metastatic CRC patients (NCT01206530), and our work suggests assessing the role of cellular iron availability in the efficacy of hydroxychloroquine in these patients. Moreover, recent work has identified compounds that directly inhibit ferritinophagy and may lead to more direct and potent growth inhibition of CRC (51).

Experimental procedures

Cell line and culture

HCT116, DLD1, MC38, HT29, and SW480 cells were maintained at 37 °C in 5% CO2 and 21% O2. Cells were cultured in Dulbecco's Modified Eagle Medium (DMEM) supplemented with 10% fetal bovine serum and 1% antibiotic/antimycotic. Constructs for DOX-inducible shRNA were generated using the Tet-pLKO-puro (Dmitri Wiederschain; Addgene plasmid #21915). shRNA primer sequences are as follows: shPRKN (F: CCGGGCTTAGACTGTTTCCACTTATCTCGAGATAAGTGGAAACAGTCTAAGCTTTTT, R: AATTAAAAAGCTTAGACTGTTTCCACTTATCTCGAGATAAGTGGAAACAGTCTAAGC), shPINK1.2 (F: CCGGGAAATCTTCGGGCTTGTCAATCTCGAGATTGACAAGCCCGAAGATTTCTTTTT, R: AATTAAAAAGAAATCTTCGGGCTTGTCAATCTCGAGATTGACAAGCCCGAAGATTTC), shPINK1.3 (F: CCGGGCCGCAAATGTGCTTCATCTACTCGAGTAGATGAAGCACATTTGCGGCTTTTT, R: AATTAAAAAGCCGCAAATGTGCTTCATCTACTCGAGTAGATGAAGCACATTTGCGGC). CRISPR KO line was generated using gRNA in LenticrisprV2 (Feng Zhang; Addgene plasmid 49535). CRISPR primer sequences are as follows: sgBNIP3 (F: CACCGATGGGATTGGTCAAGTCGGC, R: AAACGCCGACTTGACCAATCCCATC), sgNIX/BNIP3L (F: CACCGCGGCGGCGGCTCGACTAGGT. R: AAACACCTAGTCGAGCCGCCGCCGC), sgFUNDC1 (F: CACCGTAATGGGTGGCGTTACTGGC, AAACGCCAGTAACGCCACCCATTAC). NCOA4 overexpression plasmid (pIND20-NCOA4) was generously donated from Joseph D. Mancias' group. Plasmids were generated and inserted in to a lentiviral vector for stable transfection. KD was induced using 500 ng/ml of DOX for 48 h. FAC was obtained from

Sigma-Aldrich (RES20400-A7). Carbonyl cyanide m-chlorophenylhydrazone (25458), Deferoxamine mesylate (14595), Ferrostatin-1 (17729), Z-VAD(OH)-FMK (14467), Necrostatin-1 (11658), and doxycycline hyclate (14422) was obtained from Cayman Chemicals.

Mouse xenograft model

Immunocompromised (NOD.Cg-Prkdc^{scid}/J), 8- to 10-week-old mice of both were assessed, and animal work was approved by U of M IACUC. For subcutaneous xenograft studies, HCT116 and SW480 or shNT, shPINK1.2, and shPINK.13 cells were trypsinized and two million cells were implanted into the lower flanks. All treatments began on day 10 after tumors became visible. Two hundred milligrams of dox/kg diet was used to induce shRNA expression. The diet was purchased from Bioserv. Subcutaneous tumor size was measured with digital calipers at the indicated time points. Tumor volume (V) was calculated as V = 1/2(length × width2). At the endpoint, mice were sacrificed and tumors were excised. The final tumor volume and weight were measured, and tissue was used for proliferation and apoptosis assay.

Proliferation assay

Growth assays were performed using MTT (Thiazolyl Blue Tetrazolium Bromide) assays and live cell imaging. Briefly, for MTT, cells were plated down, and 24 h following plating, a Day 0 reading was taken. Cells were incubated for 45 min with MTT solution (5× concentrate stock: 5 mg/ml, in 1× PBS, pH 7.4). Media and MTT solution were then carefully aspirated followed by solubilization with dimethyl sulfoxide. Absorbance was read at 570 nm. Following the Day 0 read, the cells were treated with indicated doses and readings were taken after 24 h. Live cell imaging was done using the Cytation 5 Imaging Multi-Mode reader. Cells were plated down, treated 24 h later with indicated treatments, and immediately imaged and analyzed for cell number. Images were then taken every 24 h.

Real-time quantitative PCR

One microgram of total RNA was extracted using Trizol reagent from mouse tissues and human intestinal cell lines. RNA was reverse transcribed to complementary DNA using SuperScript III First-Strand Synthesis System (Invitrogen). Real-time PCR reactions were set up in three technical replicates for each sample. Complementary DNA gene-specific primers, SYBR green master mix was combined, and then run in QuantStudio 5 Real-Time PCR System (Applied Biosystems). The fold change of the genes was calculated using the ΔΔCt method using β-actin as the housekeeping gene. Primers are listed as follows: human PINK1 (F: GCC TCATCGAGGAAAAACAGG, R: GTCTCGTGTCCAA CGGGTC), mouse PINK1 (F: TTCTTCCGCCAGTCGGTAG, R: CTGCTTCTCCTCGATCAGCC), human PRKN/PARK2 (F: GTGTTTGTCAGGTTCAACTCCA, R: GAAAATCA-CACGCAACTGGTC), human NIX/BNIP3L (F: ATGTCGT CCCACCTAGTCGAG, R: TGAGGATGGTACGTGTTC-CAG), human BNIP3 (F: CAGGGCTCCTGGGTAGAACT, R: CTACTCCGTCCAGACTCATGC), human FUNDC1 (F: CCTCCCCAAGACTATGAAAGTGA, R: AAACACTC GATTCCACCACTG), human beta-actin/ACTB (F: CATG-TACGTTGCTATCCAGGC, R: CTCCTTAATGTCACG-CACGAT), mouse beta-actin/ACTB (F: GTGACGTT GACATCCGTAAAGA, R: GCCGGACTCATCGTACTCC).

Western blotting

Whole-cell lysate preparations were described previously (52). Whole cell lysates were prepared from cell lines by RIPA buffer. Homogenates were incubated in RIPA buffer for 15 min on ice followed by 13,000 rpm centrifugation for 15 min. Supernatants were transferred to a new tube and mixed with 5× Laemmli buffer and boiled for 5 min. Lysates containing 30 to 40 μg of protein per well were separated by SDS-PAGE, transferred onto nitrocellulose membranes, and immunoblotted overnight at 4 °C with indicated antibodies: Phospho-Ubiquitin (Ser65) (E2J6T) Rabbit mAb #62802 (Cell Signaling Technology), vinculin (E1E9V) XP Rabbit mAb #13901(Cell Signaling Technology), anti-ferritin heavy chain antibody (B-12): sc-376594 (Santa Cruz Biotechnology), anti-ferritin light chain antibody (D-9): sc-74513 (Santa Cruz Biotechnology). All the primary antibodies were used at a dilution of 1:1000. Horseradish peroxidase–conjugated secondary antibodies used were anti-rabbit and anti-mouse at a dilution of 1:2000, and immunoblots were developed using Chemidoc imaging system (ChemiDoc, Bio-Rad).

NAD/NADH measurement

NAD/NADH-Glo assays (G9071) were purchased from Promega and performed based on manufacturer instructions.

Clonogenic assays

Cells were plated in six-well plates in biological triplicates at 300 to 600 cells per well in 2 ml of media. Dox media were changed every 2 days. Assays were concluded after 10 to 15 days by fixing in −20 °C cold 100% methanol for 10 min and staining with 0.5% crystal violet 20% methanol solution for 15 min. Colonies were quantified using ImageJ or manually counted.

FerroOrange and Mito-FerroGreen measurement

The cells were washed with HBSS three times. Mito-FerroGreen working solutions (5 μmol/l) and FerroOrange working solution (1 μmol/l) were added to the cells, and the cells were incubated at 37 °C for 30 min in a 5% CO2 incubator. The supernatant was discarded, and the cells were washed with HBSS three times. Cells were then processed for flow cytometry analyses.

Mitophagy assay with flow cytometry

Cells were seeded at 100,000 cells per well in a 12-well plate. Next day, 500 ng of pCLBW cox8 EGFP mCherry (David Chan; Addgene plasmid #78520).) were transfected into the cells with Lipofectamine 2000 according to manufacturer's protocol. Cells were then treated with DOX for 48 h to induce PINK1 KD. After 48 h post transfection, cells were trypsinized

and collected for flow cytometry analyses. Cells were counterstained with DAPI to gate out dead cells. Then, mCherry-positive cells were gated, and EGFP fluorescence was assessed. Ratio of low EGFP to high EGFP was plotted as % mitophagy. Analysis was done using FlowJo software (https://www.flowjo.com/solutions/flowjo).

Metabolomics

Cells were plated at 500,000 cells per well in six-well plates or ∼1.5 million cells per 10-cm dish. At the endpoint, cells were lysed with dry-ice cold 80% methanol, and extracts were then centrifuged at 10,000*g* for 10 min at 4 °C and the supernatant was stored at −80 °C until further analyses. Protein concentration was determined by processing a parallel well/dish for each sample and used to normalize metabolite fractions across samples. Based on protein concentrations, aliquots of the supernatants were transferred to a fresh microcentrifuge tube and lyophilized using a SpeedVac concentrator. Dried metabolite pellets were resuspended in 45 μl 50:50 methanol:water mixture for LC–MS analysis.

The QqQ data were preprocessed with Agilent MassHunter Workstation Quantitative Analysis Software (https://www.agilent.com/en/promotions/masshunter-mass-spec) (B0700). Each sample was normalized by the total intensity of all metabolites to scale for loading. Finally, each metabolite abundance level in each sample was divided by the median of all abundance levels across all samples for proper comparisons, statistical analyses, and visualizations among metabolites. The statistical significance test was done by a two-tailed *t* test with a significance threshold level of 0.05.

Induced coupled plasma mass spectrometry

Metal quantifications by ICP-MS were performed as previously described (13). Briefly, tissue samples were digested with 2 ml/g total weight nitric acid (BDH Aristar Ultra) for 24 h and then digested with 1 ml/g total weight hydrogen peroxide (BDH Aristar Ultra) for 24 h at room temperature. Specimens were preserved at 4 °C until quantification of metals. Ultrapure water was used for the final sample dilution. Samples were analyzed using a PerkinElmer Nexion 2000 ICP-MS. For iron-^{57}Fe measurements, ^{57}Fe was dissolved in 0.4 mol/l H_2SO_4 to achieve a total concentration of 22.85 g/l overnight at a 37 °C shaking incubator. Cells were treated with a final concentration of 100 μM iron-^{57}Fe for 2 h and 100 μM of FAC as a control for iron-^{56}Fe. When calculating total intracellular ^{57}Fe level, background ^{57}Fe from FAC-treated cells were subtracted.

Seahorse Mito Stress test

Cells were seeded at 2×10^4 cells/well in 80 μl/well of normal growth media (DMEM with 25 mM glucose and 2 mM glutamine) in an Agilent XF96 V3 PS Cell Culture Microplate (#101085-004). To achieve an even distribution of cells within wells, plates were incubated on the bench top at room temperature for 1 h before incubating at 37 °C, 5% CO2 overnight. To hydrate the XF96 FluxPak (#102416-100), 200 μl/well of sterile water was added and the entire cartridge was incubated at 37 °C, without CO2 overnight. The following day, 1 h prior to running the assay, 60 μl/well of growth media was removed from the cell culture plate, and cells were washed twice with 200 μl/well of assay medium (XF DMEM Base Medium, pH 7.4 (#103575-100) containing 25 mM glucose (#103577-100) and 2 mM glutamine (#103579-100)). After washing, 160 μl/well of assay medium was added to the cell culture plate for a final volume of 180 μl/well. Cells were then incubated at 37 °C, without CO2 until analysis. One hour prior to the assay, water from the FluxPak hydration was exchanged for 200 μl/well of XF Calibrant (#100840-000), and the cartridge was returned at 37 °C, without CO2 until analysis. Oligomycin (100 μM), FCCP (100 μM), and rotenone/antimycin (50 μM) from the XF Cell MitoStress Test Kit (#103015-100) were reconstituted in assay medium to make the indicated stock concentrations. Twenty microliters of oligomycin was loaded into port A for each well of the FluxPak, 22 μl of FCCP into port B, and 25 μl of rotenone/antimycin into port C. Port D was left empty. The final FCCP concentration was optimized to achieve maximal respiration in each condition.

The Mito Stress Test was conducted on an XF96 Extracellular Flux Analyzer, and OCR was analyzed using Wave 2.6 software (https://www.agilent.com/en/product/cell-analysis/real-time-cell-metabolic-analysis/xf-software/seahorse-wave-desktop-software-740897). Following the assay, OCR was normalized to cell number with the CyQUANT NF Cell Proliferation Assay (C35006) from Thermo Fisher Scientific according to manufacturer's instructions.

Quantification and statistical analysis

In vitro experiments were validated in four cell lines. Each cell line experiment was performed in technical replicates for each condition and repeated at least three times with biological triplicates to ensure reproducibility. Figures show a representative biological replicate unless otherwise indicated. Blinding was performed whenever appropriate. Sample description and identification was unavailable to the core personnel during data collection and analysis. Statistical details of all experiments can be found in the figure legends. The sample numbers are mentioned in each figure legend and denote biological replicates. Statistical details are reported in figure legends. Results are expressed as the mean plus or minus the SEM for all figures unless otherwise noted. Significance between two groups was tested using a two tailed unpaired *t* test. Significance among multiple groups was tested using a one-way ANOVA. GraphPad Prism 7.0 was used for the statistical analysis. Statistical significance is described in the figure legends as: $^{*}p < 0.05$, $^{**}p < 0.01$, $^{***}p < 0.001$, $^{****}p < 0.0001$.

Data availability

Data from the metabolomic analysis are presented in Table S1. Additional information or raw data will be shared upon request addressed to the contact author.

Supporting information—This article contains supporting information.

Author contributions—B. C., C. A. L., and Y. M. S. methodology; B. C., N. K. D., I. T., R. S., C. C., J. D. M, and A. A. investigation; B. C., N. K. D., I. T., R. S., C. C., and A. A. formal analysis; B. C., C. A. L., and Y. M. S. writing–original draft; C. A. L. and Y. M. S. supervision.

Funding and additional information—This work was funded by NIH grants: R01CA148828, R01CA245546, and R01DK095201 (Y. M. S.); R37CA237421, R01CA248160, and R01CA244931 (C. A. L.); R01 DK124384 (J. D. M.); UMCCC Core Grant P30CA046592 and Center for Gastrointestinal Research P30DK034933 (Y. M. S. and C. A. L.). B. C. was supported by a Department of Defense National Defense Science and Engineering Graduate Fellowship (DoD NDSEG) and NIH Cellular and Molecular Biology Training Grant T32-GM145470. R. S. was supported by a postdoctoral fellowship from the American Physiological Society (032650). The content is solely the responsibility of the authors and does not necessarily represent the official views of the National Institutes of Health.

Conflict of interest—C. A. L. has received consulting fees from Astellas Pharmaceuticals, Odyssey Therapeutics, and T-Knife Therapeutics and is an inventor on patents pertaining to Kras-regulated metabolic pathways, redox control pathways in pancreatic cancer, and targeting the GOT1-pathway as a therapeutic approach (US Patent No: 2015126580-A1, 05/07/2015; US Patent No: 20190136238, 05/09/2019; International Patent No: WO2013177426-A2, 04/23/2015). J. D. M. reports a patent for the modulation of NCOA4-mediated autophagic targeting of ferritin (PCT/US2015/023142) issued.

Abbreviations—The abbreviations used are: CRC, colorectal cancer; DFO, deferoxamine; DMEM, Dulbecco's Modified Eagle Medium; DOX, doxycycline; ETC, electron transport chain; FAC, ferric ammonium citrate; FTL, FTN light chain; FTN, ferritin; ICP-MS, inductively-coupled plasma mass spectrometry; KD, knockdown; LIP, labile iron pool; OCR, oxygen consumption rate; OMM, outer mitochondrial membrane; pUb, phospho-ubiquitin.

References

1. Spinelli, J. B., and Haigis, M. C. (2018) The multifaceted contributions of mitochondria to cellular metabolism. *Nat. Cell Biol.* **20**, 745–754
2. Pickles, S., Vigié, P., and Youle, R. J. (2018) Mitophagy and quality control mechanisms in mitochondrial maintenance. *Curr. Biol.* **28**, R170–R185
3. Kim, I., Rodriguez-Enriquez, S., and Lemasters, J. J. (2007) Selective degradation of mitochondria by mitophagy. *Arch. Biochem. Biophys.* **462**, 245–253
4. Vara-Perez, M., Felipe-Abrio, B., and Agostinis, P. (2019) Mitophagy in cancer: a tale of adaptation. *Cells* **8**, 493
5. Jin, S. M., and Youle, R. J. (2012) PINK1- and parkin-mediated mitophagy at a glance. *J. Cell Sci.* **125**, 795–799
6. Lazarou, M., Sliter, D. A., Kane, L. A., Sarraf, S. A., Wang, C., Burman, J. L., *et al.* (2015) The ubiquitin kinase PINK1 recruits autophagy receptors to induce mitophagy. *Nature* **524**, 309–314
7. O'Flanagan, C. H., and O'Neill, C. (2014) PINK1 signalling in cancer biology. *Biochim. Biophys. Acta* **1846**, 590–598
8. Dai, K., Radin, D. P., and Leonardi, D. (2020) Deciphering the dual role and prognostic potential of PINK1 across cancer types. *Neural Regen. Res.* **16**, 659–665
9. Berthier, A., Navarro, S., Jiménez-Sáinz, J., Roglá, I., Ripoll, F., Cervera, J., *et al.* (2011) PINK1 displays tissue-specific subcellular location and regulates apoptosis and cell growth in breast cancer cells. *Hum. Pathol.* **42**, 75–87
10. Amo, T., Sato, S., Saiki, S., Wolf, A. M., Toyomizu, M., Gautier, C. A., *et al.* (2011) Mitochondrial membrane potential decrease caused by loss of PINK1 is not due to proton leak, but to respiratory chain defects. *Neurobiol. Dis.* **41**, 111–118
11. Allen, G. F. G., Toth, R., James, J., and Ganley, I. G. (2013) Loss of iron triggers PINK1/Parkin-independent mitophagy. *EMBO Rep.* **14**, 1127–1135
12. Hara, Y., Yanatori, I., Tanaka, A., Kishi, F., Lemasters, J. J., Nishina, S., *et al.* (2020) Iron loss triggers mitophagy through induction of mitochondrial ferritin. *EMBO Rep.* **21**, e50202
13. Das, N. K., Jain, C., Sankar, A., Schwartz, A. J., Santana-Codina, N., Solanki, S., *et al.* (2021) Modulation of the HIF2α-NCOA4 axis in enterocytes attenuates iron loading in a mouse model of hemochromatosis. *Blood* **139**, 2547–2552
14. Barra, J., Crosbourne, I., Wang, L., Nelson, I., Goldwag, J., Jourd'heuil, F., *et al.* (2022) DMT1-mediated endosome-mitochondria interactions regulates iron homeostasis and mitochondrial metabolism. *FASEB J.* https://doi.org/10.1096/fasebj.2022.36.S1.R5276
15. Das, A., Nag, S., Mason, A. B., and Barroso, M. M. (2016) Endosome–mitochondria interactions are modulated by iron release from transferrin. *J. Cell Biol.* **214**, 831–845
16. Ravichandran, M., Hu, J., Cai, C., Ward, N. P., Venida, A., Foakes, C., *et al.* (2022) Coordinated transcriptional and catabolic programs support iron dependent adaptation to RAS-MAPK pathway inhibition in pancreatic cancer. *Cancer Discov.* **12**, 2198–2219
17. Santana-Codina, N., Del Rey, M. Q., Kapner, K. S., Zhang, H., Gikandi, A., Malcolm, C., *et al.* (2022) NCOA4-mediated ferritinophagy is a pancreatic cancer dependency via maintenance of iron bioavailability for iron–sulfur cluster proteins. *Cancer Discov.* **12**, 2180–2197
18. Devenport, S. N., Singhal, R., Radyk, M. D., Taranto, J. G., Kerk, S. A., Chen, B., *et al.* (2021) Colorectal cancer cells utilize autophagy to maintain mitochondrial metabolism for cell proliferation under nutrient stress. *Jci Insight* **6**, e138835
19. Kane, L. A., Lazarou, M., Fogel, A. I., Li, Y., Yamano, K., Sarraf, S. A., *et al.* (2014) PINK1 phosphorylates ubiquitin to activate Parkin E3 ubiquitin ligase activity. *J. Cell Biol.* **205**, 143–153
20. Koyano, F., Okatsu, K., Kosako, H., Tamura, Y., Go, E., Kimura, M., *et al.* (2014) Ubiquitin is phosphorylated by PINK1 to activate parkin. *Nature* **510**, 162–166
21. Rojansky, R., Cha, M.-Y., and Chan, D. C. (2016) Elimination of paternal mitochondria in mouse embryos occurs through autophagic degradation dependent on PARKIN and MUL1. *Elife* **5**, e17896
22. Forkink, M., Manjeri, G. R., Liemburg-Apers, D. C., Nibbeling, E., Blanchard, M., Wojtala, A., *et al.* (2014) Mitochondrial hyperpolarization during chronic complex I inhibition is sustained by low activity of complex II, III, IV and V. *Biochim. Biophys. Acta* **1837**, 1247–1256
23. Titov, D. V., Cracan, V., Goodman, R. P., Peng, J., Grabarek, Z., and Mootha, V. K. (2016) Complementation of mitochondrial electron transport chain by manipulation of the NAD+/NADH ratio. *Science* **352**, 231–235
24. Seo, B. B., Kitajima-Ihara, T., Chan, E. K., Scheffler, I. E., Matsuno-Yagi, A., and Yagi, T. (1998) Molecular remedy of complex I defects: rotenone-insensitive internal NADH-quinone oxidoreductase of saccharomyces cerevisiae mitochondria restores the NADH oxidase activity of complex I-deficient mammalian cells. *Proc. Natl. Acad Sci. U. S. A.* **95**, 9167–9171
25. Schwartz, A. J., Goyert, J. W., Solanki, S., Kerk, S. A., Chen, B., Castillo, C., *et al.* (2021) Hepcidin sequesters iron to sustain nucleotide metabolism and mitochondrial function in colorectal cancer epithelial cells. *Nat. Metab.* **3**, 969–982
26. Li, C., Zhang, Y., Cheng, X., Yuan, H., Zhu, S., Liu, J., *et al.* (2018) PINK1 and PARK2 suppress pancreatic tumorigenesis through control of mitochondrial iron-mediated Immunometabolism. *Dev. Cell* **46**, 441–455.e8
27. Cuadros, A. M., Fernandez-Garcia, J., Planque, M., Altea-Manzano, P., Schalley, T., Vermeire, I., *et al.* (2022) In vivo CRISPR screen defines Slc25a37 as an organ-specific regulator of antioxidant metabolism in metastasis. *bioRxiv*. https://doi.org/10.1101/2022.09.03.506468
28. Wang, J., and Pantopoulos, K. (2011) Regulation of cellular iron metabolism. *Biochem. J.* **434**, 365–381
29. Reif, D. W. (1992) Ferritin as a source of iron for oxidative damage. *Free Radic. Biol. Med.* **12**, 417–427

30. Stäubli, A., and Boelsterli, U. A. (1998) The labile iron pool in hepatocytes: prooxidant-induced increase in free iron precedes oxidative cell injury. *Am. J. Physiol.* **274**, G1031–G1037
31. Shah, Y. M., and Xie, L. (2014) Hypoxia-inducible factors link iron homeostasis and erythropoiesis. *Gastroenterology* **146**, 630–642
32. Kakhlon, O., and Cabantchik, Z. I. (2002) The labile iron pool: characterization, measurement, and participation in cellular processes(1). *Free Radic. Biol. Med.* **33**, 1037–1046
33. Mancias, J. D., Wang, X., Gygi, S. P., Harper, J. W., and Kimmelman, A. C. (2014) Quantitative proteomics identifies NCOA4 as the cargo receptor mediating ferritinophagy. *Nature* **509**, 105–109
34. Fujimaki, M., Furuya, N., Saiki, S., Amo, T., Imamichi, Y., and Hattori, N. (2019) Iron supply via NCOA4-mediated ferritin degradation maintains mitochondrial functions. *Mol. Cell. Biol.* **39**, e00010–e00019
35. Weinberg, S. E., and Chandel, N. S. (2015) Targeting mitochondria metabolism for cancer therapy. *Nat. Chem. Biol.* **11**, 9–15
36. Hertweck, K. L., and Dasgupta, S. (2017) The landscape of mtDNA modifications in cancer: a tale of two cities. *Front. Oncol.* **7**, 262
37. Petros, J. A., Baumann, A. K., Ruiz-Pesini, E., Amin, M. B., Sun, C. Q., Hall, J., *et al.* (2005) mtDNA mutations increase tumorigenicity in prostate cancer. *Proc. Natl. Acad Sci. U. S. A.* **102**, 719–724
38. Narendra, D., Tanaka, A., Suen, D.-F., and Youle, R. J. (2008) Parkin is recruited selectively to impaired mitochondria and promotes their autophagy. *J. Cell Biol.* **183**, 795–803
39. Lill, R., Hoffmann, B., Molik, S., Pierik, A. J., Rietzschel, N., Stehling, O., *et al.* (2012) The role of mitochondria in cellular iron–sulfur protein biogenesis and iron metabolism. *Biochim. Biophys. Acta* **1823**, 1491–1508
40. Ye, H., and Rouault, T. A. (2010) Human iron–sulfur cluster assembly, cellular iron homeostasis, and disease. *Biochemistry* **49**, 4945–4956
41. Yang, W. S., and Stockwell, B. R. (2016) Ferroptosis: death by lipid peroxidation. *Trends Cell Biol.* **26**, 165–176
42. Yanatori, I., Richardson, D. R., Dhekne, H. S., Toyokuni, S., and Kishi, F. (2021) CD63 is regulated by iron via the IRE-IRP system and is important for ferritin secretion by extracellular vesicles. *Blood* **138**, 1490–1503
43. Poole, A. C., Thomas, R. E., Yu, S., Vincow, E. S., and Pallanck, L. (2010) The mitochondrial fusion-promoting factor mitofusin is a substrate of the PINK1/parkin pathway. *PLoS One* **5**, e10054
44. Lin, W., and Kang, U. J. (2010) Structural determinants of PINK1 topology and dual subcellular distribution. *BMC Cell Biol.* **11**, 90
45. Kimmelman, A. C., and White, E. (2017) Autophagy and tumor metabolism. *Cell Metab.* **25**, 1037–1043
46. Sowter, H. M., Ratcliffe, P. J., Watson, P., Greenberg, A. H., and Harris, A. L. (2001) HIF-1-dependent regulation of hypoxic induction of the cell death factors BNIP3 and NIX in human tumors. *Cancer Res.* **61**, 6669–6673
47. Chen, G., Han, Z., Feng, D. U., Chen, Y., Chen, L., Wu, H., *et al.* (2014) A regulatory signaling loop comprising the PGAM5 phosphatase and CK2 controls receptor-mediated mitophagy. *Mol Cell* **54**, 362–377
48. Ziegler, P. K., Bollrath, J., Pallangyo, C. K., Matsutani, T., Canli, Ö., De Oliveira, T., *et al.* (2018) Mitophagy in intestinal epithelial cells triggers adaptive immunity during tumorigenesis. *Cell* **174**, 88–101.e16
49. Lill, R., Diekert, K., Kaut, A., Lange, H., Pelzer, W., Prohl, C., *et al.* (1999) The essential role of mitochondria in the biogenesis of cellular iron-sulfur proteins. *Biol. Chem.* **380**, 1157–1166
50. Lane, D. J. R., Merlot, A. M., Huang, M. H., Bae, D. H., Jansson, P. J., Sahni, S., *et al.* (2015) Cellular iron uptake, trafficking and metabolism: key molecules and mechanisms and their roles in disease. *Biochim. Biophys. Acta* **1853**, 1130–1144
51. Fang, Y., Chen, X., Tan, Q., Zhou, H., Xu, J., and Gu, Q. (2021) Inhibiting ferroptosis through disrupting the NCOA4–FTH1 interaction: a new mechanism of action. *ACS Cent. Sci.* **7**, 980–989
52. Anderson, E. R., Taylor, M., Xue, X., Ramakrishnan, S. K., Martin, A., Xie, L., *et al.* (2013) Intestinal HIF2α promotes tissue-iron accumulation in disorders of iron overload with anemia. *Proc Natl Acad Sci U S A* **110**, E4922–E4930